Thin Solid Films 639 (2017) 29–35

Contents lists available at ScienceDirect

Thin Solid Films

journal homepage: www.elsevier.com/locate/tsf

Optical and electrical characteristics of thermally evaporated $Cu_{0.5}Ag_{0.5}InSe_2$ thin films

H.H. Güllü [a,b,*], Ö. Bayraklı [b,c,d], M. Parlak [b,c]

[a] Centeral Laboratory METU, Ankara 06800, Turkey
[b] Center for Solar Energy Research and Applications (GÜNAM), METU, Ankara 06800, Turkey
[c] Department of Physics, Middle East Technical University (METU), 06800 Ankara, Turkey
[d] Department of Physics, Ahi Evran University, 40100 Kırsehir, Turkey

ARTICLE INFO

Article history:
Received 17 March 2017
Received in revised form 12 August 2017
Accepted 14 August 2017
Available online 15 August 2017

Keywords:
Thin film
Annealing
Band gap
Electrical conductivity

ABSTRACT

In this study, optical and electrical characteristics of the $Cu_{0.5}Ag_{0.5}InSe_2$ (CAIS) polycrystalline thin films were investigated. They were deposited on soda lime glass substrates with the evaporation of pure elemental sources by using physical thermal evaporation technique at 200 °C substrate temperature. The thin films were characterized firstly in as-grown form, and then annealed under the nitrogen environment to deduce the effects of annealing on the optical and electrical properties of the deposited thin films related to their structural changes. In fact, these material properties of the CAIS thin films were studied by carrying out transmission, Hall Effect, and temperature dependent dark- and photo-conductivity measurements as a function of annealing temperature. From the optical analysis, the band gap energies were found between 1.44 and 1.51 eV for the as-grown and annealed films, respectively. The analysis of electrical conductivity showed that electrical properties of the films were dependent on the variable range hopping and thermionic emission conduction mechanisms at low temperature region and above the room temperature, respectively. Under different illumination intensities, the photo-conductivity properties of CAIS film samples were analyzed under the consideration of two-center model.
© 2017 Elsevier B.V. All rights reserved.

1. Introduction

The research on the thin film solar cells of chalcopyrite semiconductor materials has been attracted the attention to obtain high quality absorber film layer [1]. Among the family of the these materials, I–III–VI_2 set of ternary compounds are popular due to offering desired properties, such as being a direct band structure, having high absorption coefficient and their optoelectronic characteristics to be used for the possible device applications [2]. Although $CuInSe_2$ (CIS) [3] and $AgInSe_2$ (AIS) [4] are the most popular ternary chalcopyrite thin films for the use of absorber layer, their Cu-based quaternary analogies have been considered to be a potentially more suitable materials for thin film heterojunctions [5]. In fact, the world records for thin-film efficiency have been reached by using $Cu(In,Ga)Se_2$ (CIGSe) [6]. In the case of these semiconductor compounds, Cu/Ag substitution has been point of interest in the improvement of absorber material quality [7] which is mostly about shorting effect of Cu atoms due to having high diffusion coefficient [8].

The structural characteristics of the CAIS samples under the effect of annealing temperature were completed in the previous work [9]. The as-deposited films were found to be nearly stoichiometric and Se-deficiency was appeared in the composition after applying annealing processes. In addition to this change, according to measurements on surface morphology analysis, there were Se crystallites localized on the as-grown film surface and with increasing the annealing temperature, their size distribution was decreased and then they were disappeared. Both as-grown and annealed samples were found to have tetragonal structure and showed polycrystalline behavior with (112) main crystalline orientation direction at the major peak $2\theta \cong 27°$. Based on these results, in this work, the optical and electrical properties of the films were investigated depending annealing temperature.

2. Experimental details

CAIS thin films were deposited by thermal evaporation technique applying the sequential stacked layer evaporation steps by using the pure evaporation sources, Cu, Ag, In_2Se_3 and Se, on chemically cleaned glass substrates. The details of the experimental procedure in the deposition process were discussed in the previous work [9]. Following to the deposition of the thin film samples, the post-annealing treatments were applied to the films under nitrogen atmosphere in the temperature range of 300–500 °C by 100 °C step for 30 min to see the effect of annealing on the optical and electrical characteristics of thin films depending on the structural changes. On the other hand, the samples in Maltese-Cross shape were prepared for the electrical measurements by the metallic evaporation of In contact using suitable copper masks to this

* Corresponding author at: Centeral Laboratory METU, Ankara 06800, Turkey.
E-mail address: hgullu@metu.edu.tr (H.H. Güllü).

http://dx.doi.org/10.1016/j.tsf.2017.08.024
0040-6090/© 2017 Elsevier B.V. All rights reserved.

film geometry. After about 200 nm thick metal contact deposition, samples were annealed at 100 °C under nitrogen atmosphere to enhance the contact behavior.

The optical properties of the CAIS films were evaluated by transmittance measurements using Perkin-Elmer LAMBDA 45 UV/Vis spectrophotometer in the wavelength interval from 320 to 1100 nm at room temperature. For the electrical analysis, room temperature Hall Effect measurements were performed via current-voltage measurements with and without magnetic field. In this measurement, the current was supplied by Keithley 220 programmable current source, and the voltage was measured by Keithley 619 electrometer/multimeter. Walker Magnion Model FFD-4D electromagnet was used to produce magnetic field and the strength of applied magnetic field was kept constant at about 0.9 T in all measurements. In addition, temperature dependent dark- and photo-conductivity measurements were done in the temperature range of 100–420 K with 10 K temperature step. They were performed inside the Janis cryostat equipped with a cooling system by means of liquid nitrogen and the sample temperature was controlled by LakeShore 331 temperature controller. At each temperature step, Keithley 2400 sourcemeter was used to apply bias voltage to the sample and to measure the resultant current. The conductivity of the samples at each temperature point were measured under dark condition and five different illumination intensities varying in between 20 and 115 mW/cm^2.

3. Results and discussion

The analysis of optical spectra is one of the most useful tools to deduce the optical and electrical properties of the semiconductors [10]. As seen in Fig. 1, an enhancement in the transparency when CAIS thin films were subjected to annealing in between 300 and 500 °C, was observed in the optical transmission values of the films. This variation in transmission spectroscopy of the materials might be dependent on the structural transformations and possible re-ordering on the surface of the thin film with annealing process. As indicated in EDS analysis, the re-evaporation or segregation of the some constituent elements modifies the surface properties of the samples.

The absorption coefficient (α) of the samples was calculated using the transmission values by using the relation;

$$\alpha(\lambda) = \frac{1}{d} \ln\left(\frac{I_0}{I}\right) \qquad (1)$$

where $T(\lambda)$ is the normalized transmittance and d is the thickness of the thin films. The absorption coefficient of the films was calculated in the studied spectral region and they were found in between 8.5×10^4 and 7.0×10^5 cm^{-1} depending on annealing process. The low transmission of the films can be the indication of the high absorption characteristics of the films, so they can be evaluated as the absorber layer in device applications [11].

Fig. 2 depicts the relation between absorption coefficient and photon energy for the CAIS thin films in the high absorption region. According to the Tauc plots [12], the optical band gap values were determined for the as-grown and annealed films as 1.51, 1.50, 1.48 and 1.44 eV, respectively. Although the calculated bang gap values were different than some literature works [13,14], they were in a good agreement with results reported by other several researchers [15–17]. The differences with the results of the other reported works may be due to the morphological variations and deposition conditions of the films. However, the variation in the band gap values can be attributed to the observed structural modifications since the annealing temperatures were higher than the substrate temperature applied during the film growth. This change can also be evaluated in terms of the increase in the band tailing in the structure [17]. Therefore, by increasing the annealing temperature, the width of localized states tails may increase and so that it can be explained by increasing of surface states around the crystallites [15] and increase in the density of tail states adjacent to the band edge [16]. Although the spin orbit and crystal field splitting behaviors were reported in the literature for this film structure [13], valance band splitting was not observed in the measured optical spectra of these deposited films. Since it is not a general expectation for the chalcopyrite films [18,19], the nature of the single optical transition in both as-grown and annealed CAIS thin films can be related with the strain values in the structures. On the other hand, the variations in the fundamental band gap values between this experimental work and the previous studies on CAIS structure may be due to the non-cubic crystalline field effect [20].

The electrical and photo-electrical properties of the CAIS films were analyzed by means of temperature dependent conductivity under dark and illuminated situations; and room temperature Hall Effect measurements. These measurements were carried out by applying the van der Pauw method on samples deposited in Maltese-Cross geometry [21,22]. In order to determine the general behavior of the conductivity and the existent current transport mechanisms, the dark conductivity analysis were done against the ambient temperature and the experimental data was illustrated in Fig. 3. As shown in this figure, the conductivity of the samples was increasing with increasing sample temperature. The

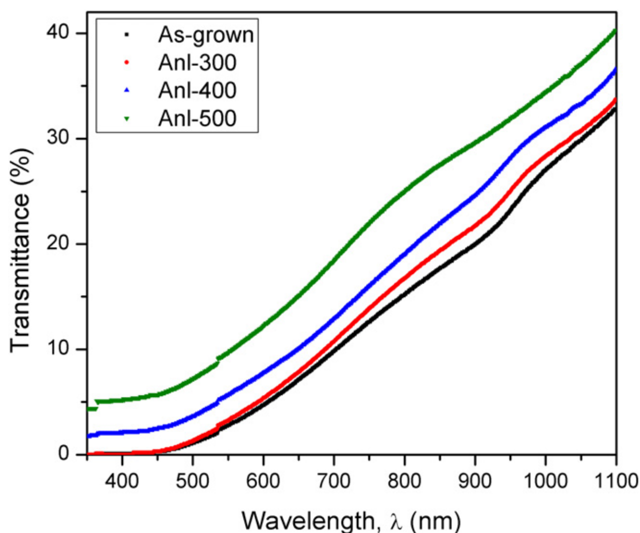

Fig. 1. The transmittance spectra of the CAIS samples.

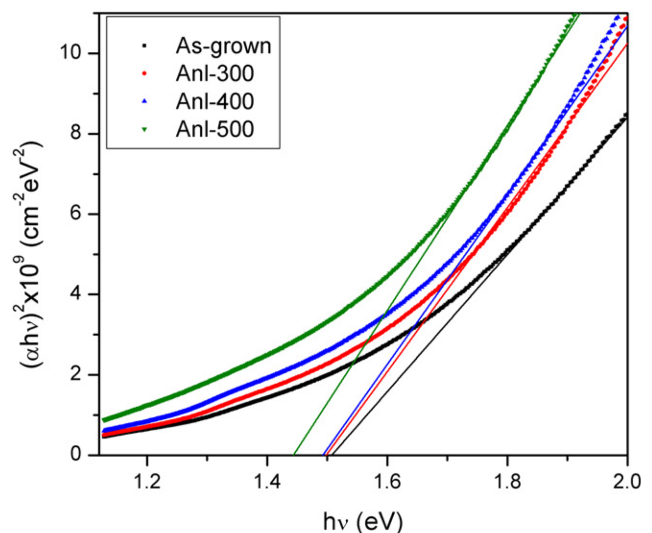

Fig. 2. The variation of $(\alpha h\nu)^2$ with the photon energy for CAIS samples.

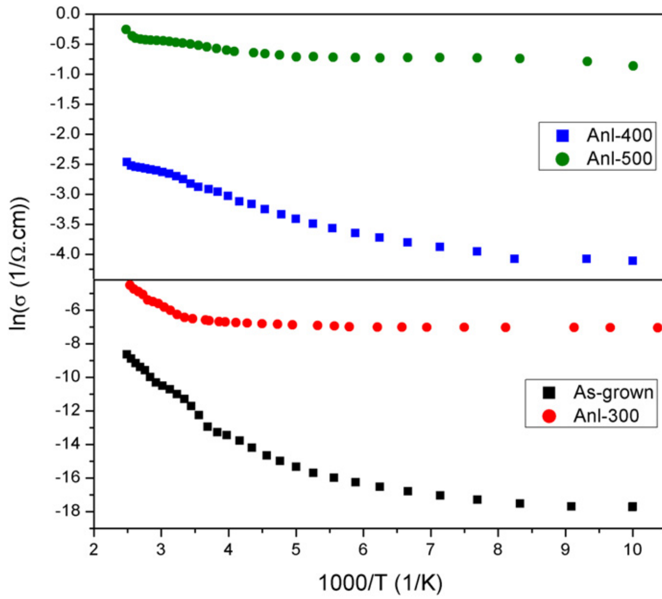

Fig. 3. Temperature-dependent electrical conductivity of as-grown and annealed CAIS films.

variation of dark conductivity with the inverse of temperature showed different linear regions for samples except film annealed at 500 °C. These variations can be taken as the indication of existence of different conduction mechanism dominating in a different temperature region with different activation energies. These energies also imply the existence of various defect levels in the forbidden band gap region [23]. On the other hand, at the last annealing step, the variation of the conductivity values was almost temperature insensitive. The semiconductor properties of the film annealed at 500 °C transformed into a degenerate form with the effect of segregation and/or re-evaporation of Se atoms in the surface structure. As observed from Fig. 3, there were three distinct slopes in the curve, two different regions at the low temperature and one at high temperature regions. Therefore, the expression of the dark conductivity of the samples was analyzed by considering the all possible conduction mechanisms. For the high temperature region where the rate of the electron emission was excessively affected by the change in the temperature, thermionic emission over the barrier was considered as a predominant conduction type. This conductivity model can be expressed as;

$$\sigma_{TE} = \sigma_{0TE} T^{1/2}\ exp\left(-{}^{E_a}/_{k_B T}\right) \tag{2}$$

where σ_{0TE} is the pre-exponential term, T is the ambient temperature, k_B is the Boltzmann constant and E_a is the activation energy [24]. The necessary fitting procedure was applied to the experimental data by using Eq. (2) to determine the thermal activation energies (see Fig. 4). Above the room temperature, the calculated energies were 264.2, 201.8 and 72.9 meV for as-grown, 300 and 400 °C annealed samples with a good agreement of correlation coefficient, R^2 value as 0.99 (Fig. 4). Since the conductivity for the sample annealed at 500 °C was almost temperature insensitive, the corresponding activation energy was calculated as 28.2 meV.

In the low temperature region, 170–270 K, the conductivity increases slowly with temperature and the temperature dependence of the electrical conductivity obeys variable range hopping (VRH) model. According to this model, the possibility of passing over the grain boundary potential barrier is not taken into consideration for charge carriers because of insufficient thermal activation energy less than kT value. Therefore, hopping can be agreed as a conduction mechanism between the localized states near the Fermi level [25,26]. As shown in Fig. 5, the conductivity of the films at this temperature region can be explained by

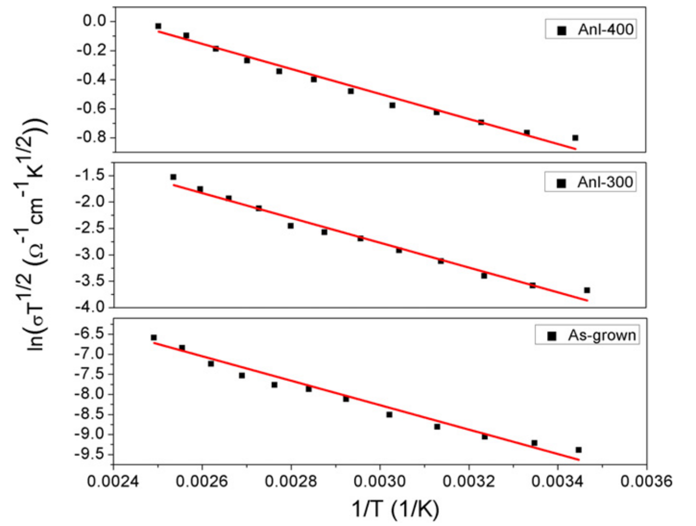

Fig. 4. Plots of $\ln(\sigma T^{1/2})$ versus T^{-1} in the high-temperature region for the as-grown and annealed at 300 and 400 °C CAIS film. Solid lines are the best fit lines.

3D Mott VRH model and the parameters related to the Mott-VRH were listed in Table 1. In this region, best fitting parameters were obtained for the conductivity values by using the expression [27]:

$$\sigma_M = {}^{\sigma_{0M}}/_{T^{1/2}}\ exp\left(\left(-{}^{T_{0M}}/_{T}\right)^{1/4}\right) \tag{3}$$

where σ_{0M} is the pre-exponential parameter and T_{0M} is the characteristic temperature constant. Their values were estimated from the straight-line nature of $\ln(\sigma_M T^{-1/2})$ versus $T^{-1/4}$ plot (Fig. 3) by Mott's equation (Eq. (3)). Moreover, σ_{0M} and T_{0M} can be defined as the following relations:

$$\sigma_{0M} = e^2 a_h^2 \nu_{ph} N(E_F) \tag{4}$$

and

$$T_{0M} = {}^{\lambda r^3}\Big/_{k_B N(E_F)} \tag{5}$$

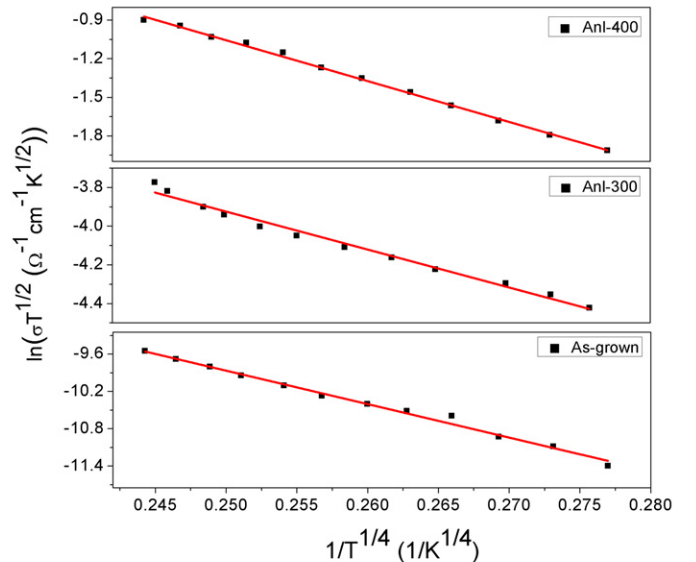

Fig. 5. Plots of $\ln(\sigma T^{1/2})$ versus $T^{-1/4}$ in the low-temperature region for the as-grown form and annealed at 300 and 400 °C CAIS film. Solid lines are the best fit lines.

Table 1
Values of the Mott VRH conduction parameters.

Sample	T_{0M} (K)	σ_{0M} ($K^{1/2}/\Omega cm$)	r (1/cm)	$N(E_F)$ (1/eV cm)	R_M (cm)	W_M (meV)	R^2	rR_M	W_M/k_BT
As-grown	8.36×10^6	3.57×10^2	3.32×10^8	9.16×10^{23}	1.56×10^{-8}	68.5	0.98	5.19	3.46
Anl-300	8.01×10^5	9.73×10^1	2.37×10^7	5.74×10^{21}	1.03×10^{-7}	38.2	0.98	2.89	1.92
Anl-400	1.67×10^5	1.23×10^1	1.62×10^6	5.29×10^{18}	1.21×10^{-6}	25.8	0.99	1.95	1.30

where e is the electronic charge, α_h is the variable hopping distance, ν_{ph} is the phonon frequency, $N(E_F)$ is the density of localized states around Fermi energy level (E_F), λ is the dimensionless constant, r is the localization radius for the wave functions of the localized states around the Fermi level. In this VRH model, T_{0M} is also related to the degree of disorder, (T_{0M}/T), in the structure [28]. In addition, ν_{ph} is generally taken ~10^{13} Hz [30]. Although the lower limit of λ was reported as to be 16 [18], it was accepted as about 18.1 which is a common usage in this analysis [29]. The other parameters in this model, average hopping distance, R_M,

$$R_M = \left({}^{9}\!/_{8\pi r k_B T N(E_F)} \right)^{1/4} \quad (6)$$

and average hopping energy, W_M;

$$W_M = {}^{3}\!/_{4\pi R_M^3 N(E_F)} \quad (7)$$

were also calculated and the obtained values listed in Table 1 were analyzed under the requirements of this model of conduction mechanism.

In the polycrystalline materials, the value of T_{0M} is a measure of degree of disorder in the structure [30]. In these deposited film samples, T_{0M} showed the decreasing behavior with increasing annealing temperature. In addition, the VRH results indicated that the calculated density of localized states near the Fermi level decreased with annealing temperature and it may be due to the effects of annealing process on the chemical bonds re-arrangements in the film structures [31]. In general, annealing process lowered the conductivity by an order of magnitude [29] and this decrease in the conductivity can be the result of the diminishing hopping states in the structure. The expected value of r and $N(E_F)$ are about 10^8 cm^{-1} and 10^{20} cm$^{-3}\cdot$eV^{-1}, respectively and these parameters listed in Table 1 were in a good agreement with the reported values [32,33]. The fitting and calculated parameters were reasonable within Mott's requirements of the localized state model as $W > k_BT$ and $rR > 1$. In fact, the value of rR indicates the degree of localization of carriers in the trap states [30].

In the low temperature region, 100–170 K, Efros-Shklovskii $T^{-1/2}$ VRH model, where Coulomb effect serves as a barrier to the conduction process, fitted the experimental data with the regression coefficient, R^2 with a value of 0.99 (Fig. 6). In this model, Mott's conduction behavior changes to the following temperature dependence under the effect of Coulomb interaction [34];

$$\sigma_{ES} = {}^{\sigma_{0ES}}\!/_{T}\; exp\left(\left(-{}^{T_{0ES}}\!/_{T} \right)^{1/2} \right) \quad (8)$$

where again σ_{0ES} is the pre-exponential term and T_{0ES} is the characteristic temperature for this model. The characteristic temperature in Efros-Shklovskii VRH model is given as,

$$T_{0ES} = {}^{\beta re^2}\!\Big/_{4\pi k_B \varepsilon \varepsilon_0} \quad (9)$$

where β is a numerical coefficient, α is exponential decay constant defined in Mott's model, ε is the dielectric constant of the material and ε_0 is the free space permittivity. In this expression, according to Shklovskii et al. [34], β can be taken as about 2.8. For the Efros-Shklovskii type of conduction, the most probable hopping distance can be defined as:

$$R_{ES} = {}^{1}\!/_{4r} \left({}^{T_{0ES}}\!/_{T} \right)^{1/2} \quad (10)$$

and also average hopping energy can be calculated from the following relation:

$$W_{ES} = {}^{1}\!/_{2} k_B T \left({}^{T_{0ES}}\!/_{T} \right)^{1/2} \quad (11)$$

According to this model, electron-electron interaction reduces the density of states at the Fermi level and therefore, creates Coulomb gap. This gap width, in 3D case, can be expressed as [35]:

$$\Delta_{ES} = {}^{e^3 N(E_F)^{1/2}}\!\Big/_{(4\pi\varepsilon\varepsilon_0)^{3/2}} \quad (12)$$

In this phenomenon, the occupied states are separated from empty states by the gap equal to Δ_{ES} [34]. The obtained values of the VRH parameters were given in Table 2. According to these results, this model exactly matched with the experimental conductivity behavior at this temperature interval, and also the calculated values showed that the gap width Δ_{ES} is comparable to the hopping energy W_{ES} because of Coulomb effect. The characteristic Efros–Shklovskii parameters had the same systematic variation with the Mott parameters when compared with each other. Calculated average hopping distance and average hopping energy values for Efros–Shklovskii model were lower than those for Mott model as observed in the literature works [36,37]. This observation supported the possibility of a crossover in VRH mechanism from the Mott type to the Efros-Shklovskii type [38].

Hall Effect measurements were performed for all CAIS samples under the constant magnetic field strength of about 0.9 T at room temperature. The sign of Hall-voltage showed that all the samples were p-type and their conductivity behaviors were also confirmed by

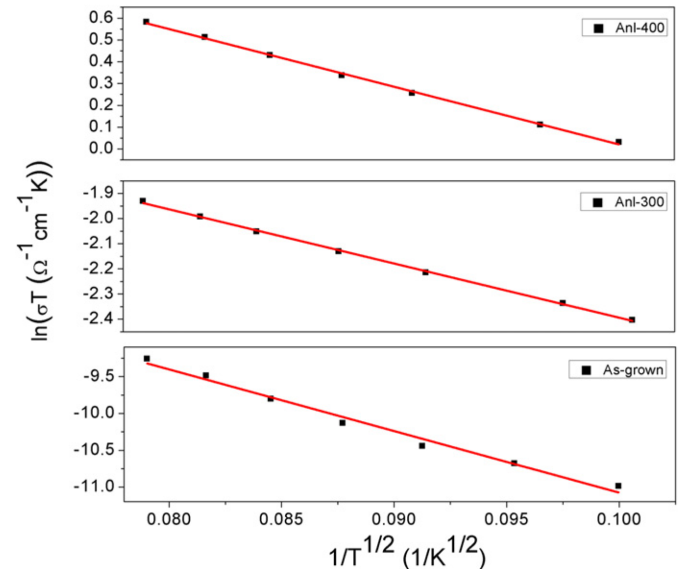

Fig. 6. Plots of ln(σT) versus $T^{-1/2}$ in the high-temperature region for the as-grown and annealed at 300 and 400 °C CAIS film. Solid lines are the best fit lines.

Table 2
Values of the Efros-Shklovskii VRH conduction parameters.

Sample	T_{0ES} (K)	σ_{0ES} (K/Ωcm)	R_{ES} (cm)	W_{ES} (meV)	Δ_{ES} (meV)	R^2	W_{ES}/k_BT
As-grown	7.06×10^3	7.05×10^{-2}	5.77×10^{-9}	39.7	48.8	0.99	3.84
Anl-300	5.76×10^2	9.54×10^{-1}	1.95×10^{-8}	11.4	6.1	0.99	1.10
Anl-400	5.58×10^2	1.61×10^1	3.33×10^{-7}	11.2	5.7	0.99	1.08

hot probe method. Moreover, the room temperature carrier concentration values of the as-grown film and annealed films annealed were found between 1.89×10^{16} and 3.56×10^{18} cm^{-3}; and the Hall mobility values were obtained as in the range of 0.33–3.58 cm^2/V·s, respectively.

The photoconductivity characteristics of the samples were also investigated with conductivity measurements under five different illumination intensities. Fig. 7 shows the temperature dependence of dark current (I_{dark}) and photocurrent (I_{ph}) in between 100 and 420 K. These plots also present the increasing behavior of the conductivity values with increase in illumination intensity at each temperature step. As seen in Fig. 7, the photoconductivity values were greater than the dark conductivity values, and it can be taken as the contribution of the photo-carriers to the conduction. Moreover, the conductivity of the samples increases with increasing the illumination intensity. The variation of the photo-conductivity values was investigated by photosensitivity calculations in which it was used as a basic parameter for photo-conductive materials [39,40]. The photosensitivity analysis of these CAIS films illustrated that there was a decreasing behavior with increasing annealing temperature. On the other hand, the change in the ratio of dark and illuminated currents depending on the applied voltage increased with the increasing illumination intensity for all samples. In order to study the carrier recombination characteristics in the CAIS films, the relation between the photocurrent and photoexcitation intensity was analyzed. The power exponent coefficient of proportionality for each film at different ambient temperature was calculated. The corresponding analysis for all CAIS films at the absolute temperatures between 100 and 400 K with 50 K increments were shown in Fig. 8. The variation with the illumination intensities has the characteristic of $I_{pc} \propto \Phi^{\gamma}$ where the exponent, γ, is a distinctive indicator of the non-equilibrium carriers and determines the type of the recombination mechanism [41]. The photo-conductivity dependence of light intensity and temperature was calculated according to two-center model [42]. At low temperatures this coefficient was below 0.5 for as-grown films, and around 1.0 for the films annealed at 300 and 400 °C, and it was almost 0.5 for the films annealed at 500 °C. Then, the γ values increased up to 1.0 for as-grown and to 1.2 for the films annealed at 300 °C. In addition, it reached to about 2.0 for the films annealed at 400 and 500 °C. According to the two-center recombination model; as-grown and 500 °C annealed CAIS thin films change its behavior from sublinear to supralinear with the variation in the sample temperature; however, the other annealed films were found in the supralinear photoconductivity behavior at all temperatures. This increasing behavior of the exponent γ values with increasing ambient temperature confirmed the longer lifetimes for free carriers and stronger recombination process at the film surface [43].

4. Conclusion

The aim of this study was to determine the optical and electrical properties of the CAIS thin films under the effect of post-thermal annealing as a continuation of the work on the structural characterization. Although the transmittance measurements were performed using the same samples which were used in the previous work, for the electrical characterization the samples prepared in the Maltese cross-shaped geometry in the same deposition process were used and also In-Ohmic contact deposition were carried out on these films after applying each annealing processes. The studies on the optical characteristics of the films revealed that the transmission values of the all films were found in the limit of 40% and the absorption coefficient of these films were obtained in the order of 10^5 cm^{-1}. In the band structure analysis, the band

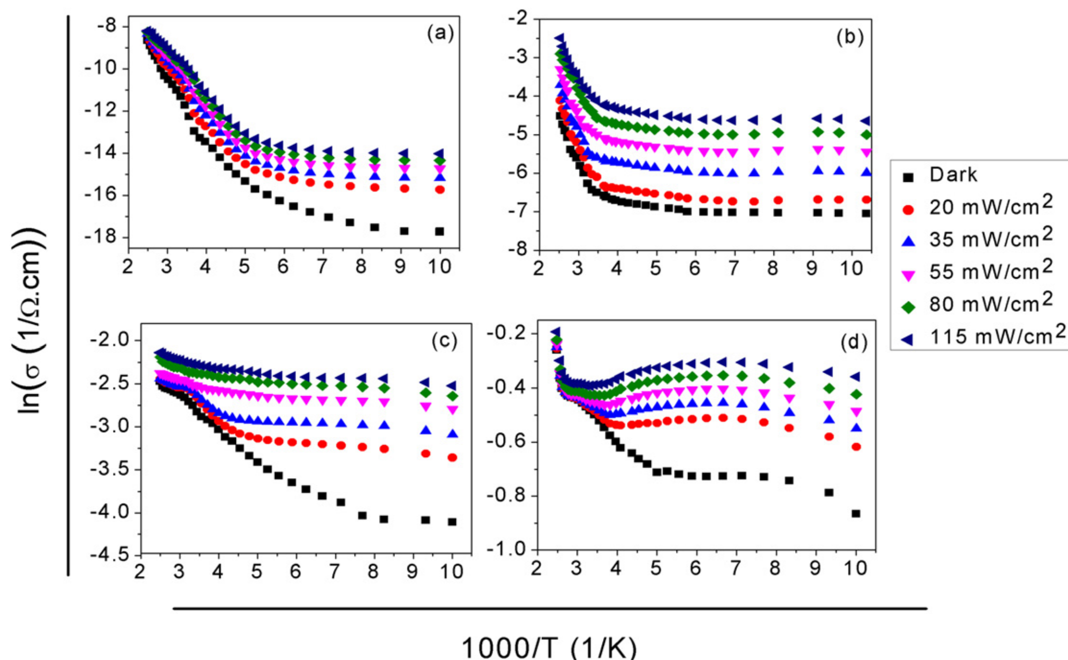

Fig. 7. The variation of the photoconductivity with temperature and illumination intensity for CAIS films (a) as-grown, (b) annealed at 300 °C, (c) annealed at 400 °C, (d) annealed at 500 °C.

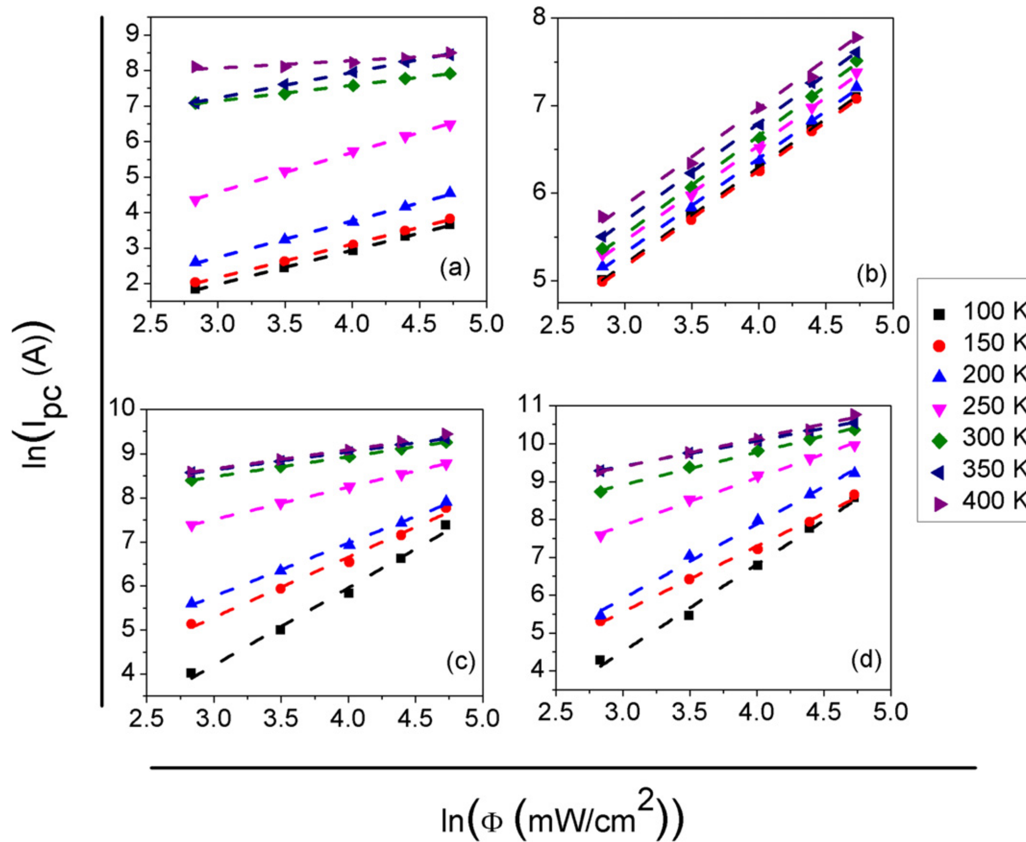

Fig. 8. The variation of the photocurrent as a function of illumination intensity for CAIS films (a) as-grown, (b) annealed at 300 °C, (c) annealed at 400 °C, (d) annealed at 500 °C.

gap energies were for the as-grown and annealed films between 1.44 and 1.51 eV. The temperature dependent dark conductivity measurements exhibited that the electrical properties of the films were dependent on the same conduction mechanisms even if annealing process was applied. At low temperature region, VRH was found to be main conduction mechanism; however thermal emission became dominant above the room temperature. Then, by applying five different illumination intensities on the sample, the photoconductivity characteristics were investigated. With further analysis, photoconductivity behavior of the films was found in a good agreement with the two-center recombination model and so that the supra-linear photoconductivity was obtained from the relation between the photocurrent and the illumination intensity. From the Hall Effect and hot probe measurements, all of the samples revealed p-type conductivity behavior. As a result of the room temperature Hall Effect measurements, improvement in both of Hall mobility and hole concentration values were observed depending on increase in the annealing temperature.

References

[1] Y. Hamakawa, Thin-film Solar Cells: Next Generation Photovoltaics and Its Applications, Springer, New York, 2004.
[2] B.J. Stanbery, Copper indium selenides and related materials for photovoltaic devices, Crit. Rev. Solid State Mater. Sci. 27 (2002) 73–117.
[3] A. Rockett, R.W. Birkmire, $CuInSe_2$ for photovoltaic applications, J. Appl. Phys. 70 (1991) R81–R97.
[4] P.P. Ramesh, O.M. Hussain, S. Uthanna, B.S. Naidu, P.J. Reddy, Photovoltaic performance of p-$AgInSe_2$/n-CdS thin film heterojunctions, Mater. Lett. 34 (1998) 217–221.
[5] J.L. Shay, J.H. Wernick, Ternary Chalcopyrite Semiconductors: Growth, Electronic Properties, and Application, Pergamon Press, Great Britain, 1975.
[6] S. Adachi, Earth-Abundant Materials for Solar Cells: Cu_2-II-IV-VI_4 Semiconductors, John Wiley & Sons, Ltd., United Kingdom, 2015.
[7] J.H. Boyle, B.E. McCandless, N. Shafarman, R.W. Birkmire, Structural and optical properties of (Ag,Cu)(In,Ga)Se_2 polycrystalline thin film alloys, J. Appl. Phys. 115 (2014) 223504.
[8] J.M. Joseph, C.S. Menon, Electrical conductivity, optical absorption and structural studies in $AgInSe_2$ thin films, Semicond. Sci. Technol. 11 (1996) 1668–1671.
[9] H.H. Gullu, M. Parlak, Structural characteristics of thermally evaporated $Cu_{0.5}Ag_{0.5}InSe_2$ thin films, Mater. Res. Exp. 3 (2016) 055901.
[10] S. Adachi, Optical Constants of Crystalline and Amorphous Semiconductors: Numerical Data and Graphical Information, Kluwer Academic, Boston/Drodrecht/London, 1999.
[11] S. Fonash, Solar Cell Device Physics, Elsevier Inc., USA, 2010.
[12] J. Tauc, Optical Properties of Solids, North Holland Publishing Co., Amsterdam, 1970.
[13] G.V. Rao, G.H. Chandra, P.S. Reddy, O.M. Hussain, K.T.R. Reddy, S. Uthanna, Optical absorption studies on polycrystalline $Cu_{0.5}Ag_{0.5}InSe_2$ thin films, Vacuum 67 (2002) 293–298.
[14] A.R. Aquino, S.A. Little, S. Marsillac, R. Collins, A. Rockett, Identification of defect levels in $Cu_xAg_{1-x}InSe_2$ thin films via photoluminescence, Conference Record of the IEEE Photovoltaic Specialists Conference 2011, pp. 003532–003536.
[15] A.S. Soltan, Thermal annealing dependence of the optical and electrical properties of amorphous $Se_{79}Te_{15}Sb_6$ thin films, Appl. Phys. A Mater. Sci. Process. 80 (2005) 117–121.
[16] A.A. Gahamdi, S.A. Khan, S. Al-Heniti, F.A. Al-Agel, M. Zulfequar, Annealing and laser irradiation effects on optical constants of $Ga_{15}Se_{85}$ and $Ga_{15}Se_{83}In_2$ chalcogenide thin films, Curr. Appl. Phys. 11 (2011) 315–320.
[17] M.M. Hafiz, A.A. Othman, M.M. El-Nahass, A.T. Al-Motasem, Composition and thermal-induced effects on the optical constants of $Ge_{20}Se_{80-x}Bi_x$ thin films, Physica B 390 (2007) 348–355.
[18] H. Karaagac, M. Kaleli, M. Parlak, Characterization of $AgGa_{0.5}In_{0.5}Se_2$ thin films deposited by electron-beam technique, J. Phys. D: Appl. Phys. 42 (2009) 165413.
[19] H. Karaagac, M. Parlak, Investigation of physical properties of quaternary $AgGa_{0.5}In_{0.5}Te_2$ thin films deposited by thermal evaporation, J. Alloys Compd. 503 (2010) 468–473.
[20] Y. Wu, G. Chen, S.H. Wei, M. Al-Jassim, Y. Yan, Unusual nonlinear strain dependence of valence-band splitting in ZnO, Phys. Rev. B 86 (2012) 155205.
[21] L.J. van der Pauw, A method of measuring the resistivity and Hall coefficient on lamellae of arbitrary shape, Philips Tech. Rev. 20 (1958) 220.
[22] L.J. van der Pauw, A method of measuring specific resistivity and Hall effect of discs of arbitrary shape, Philips Res. Rep. 13 (1958) 1.
[23] P.J. George, A. Sanchez, P.K. Nair, M.T.S. Nair, Doping of chemically deposited intrinsic CdS thin films to n type by thermal diffusion of indium, Appl. Phys. Lett. 66 (1995) 3624.
[24] T. Colakoglu, M. Parlak, Electrical and photoelectrical properties of Ag–In–Se thin films evaporated by e-beam technique, J. Phys. D. Appl. Phys. 42 (2009), 035416.
[25] N.F. Mott, E.A. Davis, Electronic Processes in Non-crystalline Materials, Clarendon Press, Oxford, 1971.
[26] J. Singh, Electronic and Optoelectronic Properties of Semiconductor Structures, Cambridge University Press, New York, 2003.

[27] R. Singh, R.P. Tandon, G.S. Singh, S. Chandra, Evaluation of Mott's parameters in BF^{-} doped polypyrrole films, Philos. Mag. B 66 (1992) 285–291.
[28] A. Bozkurt, M. Parlak, C. Ercelebi, L. Toppare, Conduction mechanism in H-type polysiloxane-polypyrrole block copolymers, J. Appl. Polym. Sci. 85 (2002) 52–56.
[29] D.K. Paul, S.S. Mitra, Evaluation of Mott's parameters for hopping conduction in amorphous Ge, Si, and Se-Si, Phys. Rev. Lett. 31 (1973) 1000.
[30] A.L. Dawar, K.V. Ferdinand, C. Jagdish, P. Kumar, P.C. Mathur, Electrical properties of Te-rich, Cd-rich and hydrogen-exposed polycrystalline CdTe thin films, J. Phys. D. Appl. Phys. 16 (1983) 2349–2360.
[31] M.M.A. Imran, O.A. Lafi, M. Abu-Samak, Effect of thermal annealing on some electrical properties and optical band gap of vacuum evaporated $Se_{65}Ga_{30}In_5$ thin films, Vacuum 86 (2012) 1589–1594.
[32] R.M. Hill, Hopping conduction in amorphous solids, Philos. Mag. 24 (1971) 1307–1325.
[33] M. Pollack, A percolation treatment of DC hopping conduction, J. Non-Cryst. Solids 8–10 (1972) 486–491.
[34] B.I. Shklovskii, A.L. Efros, Electronic Properties of Doped Semiconductors, Springer, Heidelberg, 1984.
[35] A.L. Efros, Coulomb gap in disordered systems, J. Phys. C Solid State Phys. 9 (1976) 2021.
[36] R. Rosenbaum, Crossover from Mott to Efros-Shklovskii variable-range-hopping conductivity in In_xO_y films, Phys. Rev. B 44 (1991) 3599.
[37] E. Coskun, H.H. Gullu, M. Parlak, C. Ercelebi, Study on the structural and electrical properties of sequentially deposited Ag–Ga–In–Te thin films, J. Low Temp. Phys. 178 (2015) 162–173.
[38] Y.L. Huang, S.P. Chiu, Z.X. Zhu, Z.Q. Li, J.J. Lin, Variable-range-hopping conduction processes in oxygen deficient polycrystalline ZnO films, J. Appl. Phys. 107 (2010), 063715.
[39] R. Chander, R. Thangaraj, Photoconductivity studies of Te-substituted Sn-Sb-Se semiconducting films, Appl. Phys. A Mater. Sci. Process. 114 (2014) 619–624.
[40] A. Kumar, S. Goel, S.K. Tripathi, Steady-state and transient photoconductivity in amorphous thin films of Ge_xSe_{100-x}, Phys. Rev. B 38 (1988) 13432.
[41] R.H. Bube, Photoconductivity of Solids, Interscience, New York, 1960.
[42] R.H. Bube, Photoelectronic Properties of Semiconductors, Cambridge University Press, Great Britain, 1992.
[43] H. Karaagac, M. Parlak, Deposition of $AgGaS_2$ thin films by double source thermal evaporation technique, J. Mater. Sci. Mater. Electron. 22 (2011) 1426–1432.